Available online at www.sciencedirect.com
ScienceDirect
Journal of Nuclear Materials 374 (2008) 129–137
journal of nuclear materials
www.elsevier.com/locate/jnucmat

# Updated solution for stresses and displacements in TRISO-coated fuel particles

Gregory K. Miller *, David A. Petti, John T. Maki, Darrell L. Knudson

*Idaho National Laboratory, P.O. Box 1625, Idaho Falls, ID 83415-3855, United States*

Received 3 April 2007; accepted 9 July 2007

**Abstract**

A closed-form solution for stresses and displacements in TRISO-coated fuel particles of a high temperature reactor has been updated to enhance its application in fuel particle analysis. The modified solution is applied incrementally through irradiation, which allows the material properties and irradiation temperature to change with time. It also removes the restriction in the original solution that Poisson's ratio in creep for the pyrocarbon layers be set to 0.5. It is presented in a manner that would enable its application to a system of any number of coating layers, not just the three layers of a TRISO-coated particle. The solution has been implemented in the PARFUME fuel performance code, where it has been demonstrated to perform efficiently in particle failure probability determinations.
Published by Elsevier B.V.

## 1. Introduction

The coating layers of a TRISO-coated fuel particle consist of an inner pyrolytic carbon (IPyC) layer, a silicon carbide (SiC) layer, and an outer pyrolytic carbon (OPyC) layer. These layers surround the fuel kernel and buffer, and act as a pressure vessel for fission product gases as well as a barrier to the migration of other fission products (Fig. 1). Fuel performance codes, such as Idaho National Laboratory's PARFUME, determine stresses in these coating layers so that particles can be evaluated for failure during irradiation, and also calculate displacements that are used in determining particle temperatures and gas pressure.

Early models of coated fuel particles used iterative numerical procedures to include the effects of pyrocarbon creep and swelling in determining stresses in the coating layers [1,2]. Iterative procedures, though, are cumbersome to apply when treating statistical variations in Monte Carlo sampling of large particle populations. Bongartz simplified the stress analysis with a closed-form solution based on the assumption of a rigid SiC layer, which enhanced the speed of Monte Carlo calculations [3]. Miller and Bennett subsequently derived a closed-form solution for a three-layer particle that allows for flexibility in the SiC layer [4] and is well suited for Monte Carlo simulations.

The solution of Ref. [4] includes stresses that result from irradiation-induced creep and swelling of the PyC layers, internal pressure due to fission gas release, external ambient pressure, and elastic behavior of all three coating layers. As formulated, it solves for stresses at a point in time in a single step that starts at the beginning of irradiation. Though this makes for a very efficient solution, it is subject to a number of limitations. It does not allow material properties, such as the elastic moduli or creep coefficients of the coating layers, to change with time (or fluence). Nor does it address situations where the irradiation temperature changes with time. A changing temperature significantly affects the stress evolution over time, and induces differential thermal expansion stresses in the layers. A further limitation is the simplifying assumption that Poisson's ratio in creep for the pyrocarbons is 0.5. The stresses and displacements in the coating layers are sensitive to this parameter, and experimental evidence suggests

* Corresponding author. Tel.: +1 208 526 0360; fax: +1 208 526 2930.
*E-mail address:* GregoryK.Miller@inl.gov (G.K. Miller).

0022-3115/$ - see front matter Published by Elsevier B.V.
doi:10.1016/j.jnucmat.2007.07.016

**Nomenclature**

| | |
|---|---|
| $\varepsilon$ | strain (μm/μm) |
| $t$ | neutron fluence ($10^{25}$ n/m$^2$, $E > 0.18$ MeV) |
| $E$ | modulus of elasticity of a coating layer (MPa) |
| $c$ | irradiation-induced creep coefficient of a pyrocarbon layer (MPa n/m$^2$)$^{-1}$ |
| $\sigma$ | stress (MPa) |
| $\mu$ | Poisson's ratio of a coating layer |
| $v$ | Poisson's ratio in creep for a pyrocarbon layer |
| $S$ | swelling strain rate (n/m$^2$)$^{-1}$ |
| $\overline{S}$ | average swelling strain rate over a time increment (n/m$^2$)$^{-1}$ |
| $u$ | radial displacement (μm) |
| $r$ | radial coordinate (μm) |
| $p$ | radial stress (or pressure) acting on the inner surface of a coating layer (MPa) |
| $q$ | radial stress (or pressure) acting on the outer surface of a coating layer (MPa) |
| $\alpha$ | thermal expansion coefficient of a coating layer ($K^{-1}$) |
| $\overline{\alpha}$ | average thermal expansion coefficient over a time increment ($K^{-1}$) |
| $\dot{T}$ | rate of change in temperature (K ($10^{25}$n/m$^2$)$^{-1}$) |

*Subscripts*

| | |
|---|---|
| r | radial |
| t | tangential |
| I | IPyC layer |
| S | SiC layer |
| O | OPyC layer |
| a | inner surface of a coating layer |
| b | outer surface of a coating layer |
| B | buffer |
| k | kernel |

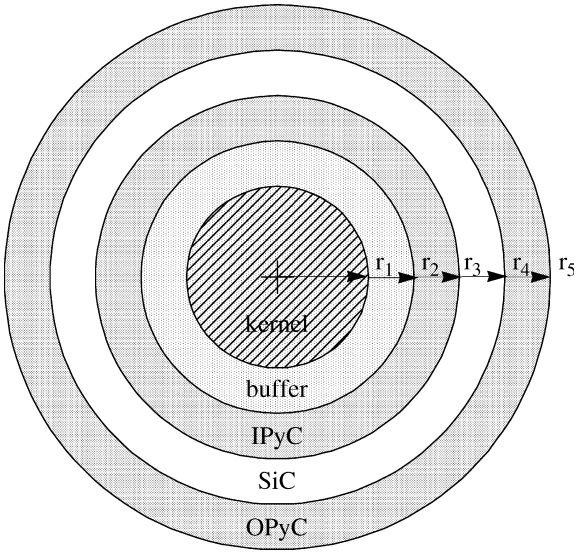


Fig. 1. Typical TRISO-coated particle geometry.

that the actual value could start at 0.5 but decrease suddenly with irradiation [5]. It is desirable, therefore, to allow this parameter to assume any realistic value that could change with time. The solution has been extended herein to remove all of these limitations. Additionally, the solution is presented in a manner that would enable its application to a particle having any number of coating layers, not just the three layers of a TRISO-coated particle. The basic approach used is to resolve the solution into time increments, using stresses calculated at the end of an increment as initial conditions for the following increment. The solution remains closed-form, so does not require iteration to reach convergence, and has been proven to perform effectively in simulations of large particle populations in the PARFUME code.

## 2. Theory and derivation

### 2.1. Governing equations and solution

As in Ref. [4], equations for the two components of strain in the spherical geometry of a TRISO particle, including Poisson effects, are as follows (see Nomenclature for definitions):

$$\frac{\partial \varepsilon_r}{\partial t} = \frac{1}{E}\left(\frac{\partial \sigma_r}{\partial t} - 2\mu\frac{\partial \sigma_t}{\partial t}\right) + c(\sigma_r - 2v\sigma_t) + S_r + \alpha_r \dot{T}, \tag{1}$$

$$\frac{\partial \varepsilon_t}{\partial t} = \frac{1}{E}\left((1-\mu)\frac{\partial \sigma_t}{\partial t} - \mu\frac{\partial \sigma_t}{\partial t}\right) + c[(1-v)\sigma_t - v\sigma_r] + S_t + \alpha_t \dot{T}. \tag{2}$$

Strains due to anisotropic thermal expansion have been added to accommodate temperature changes that may occur during irradiation. These equations incorporate the secondary creep (creep strain rate is proportional to the stress) that characterizes the pyrocarbon material. The strain–displacement relationships and equilibrium requirements for a spherical system complete the description of the behavior of the pyrocarbon layers [6]:

$$\varepsilon_r = \frac{\partial u}{\partial r}, \tag{3}$$

$$\varepsilon_t = \frac{u}{r}, \tag{4}$$

$$\frac{\partial \sigma_r}{\partial r} + \frac{2}{r}(\sigma_r - \sigma_t) = 0. \tag{5}$$

The same equations describe behavior of the SiC layer except that creep and swelling terms are generally omitted. As before, the following solution is assumed:

$$u(r,t) = \sum_{i=0}^{\infty} u_i(r) t^i, \tag{6}$$

$$\sigma_r(r,t) = \sum_{i=0}^{\infty} \sigma_{ri}(r) t^i, \tag{7}$$

$$\sigma_t(r,t) = \sum_{i=0}^{\infty} \sigma_{ti}(r) t^i, \tag{8}$$

where $i$ is the term number and is an exponent on time $t$.

The $t^0$ term is included in these summations to accommodate the presence of internal or external pressures at time zero. In Ref. [4], the simplification of setting Poisson's ratio in creep ($\nu$) equal to 0.5 was made, which would make the pyrocarbons incompressible as they creep. Material properties used in the PARFUME code for the coating layers are generally obtained from Ref. [7], which recommends the use of 0.5 for $\nu$ but acknowledges that some other sources prescribe a lower value. Calculations have shown that a lower value can significantly lower the stresses in the coating layers. This is demonstrated in Fig. 2, where the tangential stress history at the inner surface of the SiC layer in a representative fuel particle has been calculated for three values of $\nu$ (0, 0.25, and 0.5). The results show that the stress magnitude was lowered by approximately 50% when $\nu$ was reduced from 0.5 to 0. The tangential stresses in the coating layers reach a much larger magnitude than the radial stresses. Additionally, the magnitude of the tangential stress in the layers is largely controlled by the strains in the tangential direction [8]. Referring to Eq. (2), it is evident then that a value of zero for $\nu$ would give the largest creep effect, and therefore the largest reduction in stress due to creep stress relaxation.

The full physical range for $\nu$ is 0–0.5, covering the range from maximum volumetric change to zero volumetric change. Therefore, the derivation is modified to allow any value from 0 to 0.5 for this parameter. With the incremental solution derived here, the parameter $\nu$ can be varied as desired throughout irradiation. Incorporating this generalization into the derivation modifies Eqs. (11) and (12) of Ref. [4] as follows:

$$\frac{d^2 u_i}{dt^2} + \frac{2}{r}\frac{du_i}{dr} - \frac{2}{r^2}u_i = \frac{2}{Er}(1-2\mu) f_i + \frac{2}{r} c(1-2\nu)\frac{f_{i-1}}{i}, \tag{9}$$

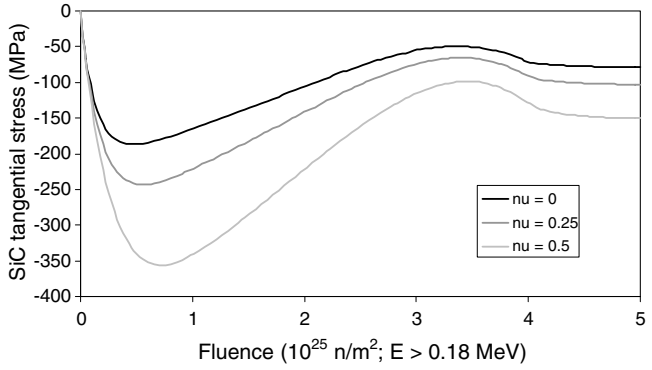


Fig. 2. Effects of variations in the parameter $\nu$ (Poisson's ratio in creep) on the SiC tangential stress.

$$f_{i+1} = -\frac{cE(1-\nu)}{(1-\mu)}\frac{f_i}{(i+1)} + \frac{E[(S_r)_i - (S_t)_i + (\alpha_r \dot{T})_i - (\alpha_t \dot{T})_i]}{(1-\mu)(i+1)}, \text{ where } f_0 = 0. \tag{10}$$

In these expressions, the functions for swelling and thermal expansion strain rates have been expanded into series, such as $S_r = \sum (S_r)_i t^i$. As before, a function $F(t)$ is defined as follows:

$$F(t) = \sum_{i=1}^{\infty} f_i t^i. \tag{11}$$

This function, which is solved for in Section 2.3, is needed for determining stresses in the coating layers.

The displacement equation of Ref. [4] becomes:

$$u_i = A_i r + \frac{B_i}{r^2} + \left[\frac{2(1-2\mu)}{3E} f_i + \frac{2c(1-2\nu)}{3i} f_{i-1}\right] r \ln r, \tag{12}$$

while the following equation remains unchanged:

$$\sigma_{ti}(r) - \sigma_{ri}(r) = \frac{3(r_a r_b)^3}{r^3(r_a^3 - r_b^3)}\left[p_i - q_i - \frac{2}{3} f_i \ln\frac{r_a}{r_b}\right] + \frac{f_i}{3}. \tag{13}$$

Following the process of Ref. [9], Eqs. (12) and (13) can be used to develop the following equation for radial displacement at any time and radial location in a spherical shell that exhibits swelling and creep in addition to normal elastic behavior:

$$u(r,t) = K_1 p + K_2 q + K_3 \int pc\,dt + K_4 \int qc\,dt + K_5 \int (S_r + \alpha_r \dot{T})\,dt + K_6 \int (S_t + \alpha_t \dot{T})\,dt + K_7 F(t), \tag{14}$$

where the coefficients $K_i$, which are dependent on the geometry and properties of the layer and on the radius $r$, are given by Eqs. (A.1)–(A.7) of the Appendix. It is noted that the coefficient $K_7$ vanishes at the layer surfaces. The stresses (or pressures) $p$ and $q$ acting at the layer surfaces are treated as positive outward. If the layer does not creep or swell (such as the SiC layer), this equation reduces to that of a pressurized thick elastic shell.

The series solution of Eqs. (6)–(8) evolves into a closed form solution for the displacement in Eq. (14) and subsequently for stresses in Eqs. (34) and (35) below. While it may be possible to attain the solution by other means, the key is to produce Eqs. (14), (34) and (35), since these give the general solution at any time for the displacement and stresses in a single layer. From these, the solution for any multi-layered particle can be derived. It is noted that the contribution to displacement from the integral terms of Eq. (14) can grow steadily with time as energy is imparted to the layer. In a single layer, these displacements could grow without bound until failure is reached. Deformations in the three-layer coating system of a

TRISO-coated particle, though, are controlled by the restraint of the stiff SiC layer. Eq. (14) is applied below to the four shell surfaces located at the two interfaces ($r = r_3, r_4$) of the TRISO-coated particle. The IPyC and OPyC layers are assumed to exhibit secondary creep and anisotropic swelling, and all three layers are allowed to exhibit anisotropic thermal expansion.

IPyC outer surface:

$$u_I = a_1 p + a_2 \sigma_{rI} + a_3 \int p c_I \, dt + a_4 \int \sigma_{rI} c_I \, dt + a_5 \int (S_{rI} + \alpha_{rI} \dot{T}_I) \, dt + a_6 \int (S_{tI} + \alpha_{tI} \dot{T}_I) \, dt. \quad (15)$$

SiC inner and outer surfaces:

$$u_I = b_1 \sigma_{rI} + b_2 \sigma_{rO} + b_3 \int \alpha_{rS} \dot{T}_S \, dt + b_4 \int \alpha_{tS} \dot{T}_S \, dt. \quad (16)$$

$$u_O = c_1 \sigma_{rI} + c_2 \sigma_{rO} + c_3 \int \alpha_{rS} \dot{T}_S \, dt + c_4 \int \alpha_{tS} \dot{T}_S \, dt. \quad (17)$$

OPyC inner surface:

$$u_O = d_1 \sigma_{rO} + d_2 q + d_3 \int \sigma_{rO} c_O \, dt + d_4 \int q c_O \, dt + d_5 \int (S_{rO} + \alpha_{rO} \dot{T}_O) \, dt + d_6 \int (S_{tO} + \alpha_{tO} \dot{T}_O) \, dt, \quad (18)$$

where the coefficients $a_j$, $b_j$, $c_j$, and $d_j$ are determined by substituting the appropriate radii and material properties into the expressions for $K_i$. If the swelling or thermal expansion in a layer is isotropic, the radial and tangential components can simply be set equal.

### 2.2. Radial stresses at SiC surfaces

The radial stresses at the interfaces are solved by equating displacements at the interfaces and differentiating the resulting equations with respect to $t$. This results in two simultaneous differential equations as follows:

$$\frac{d\sigma_{rO}}{dt} - B_2 \sigma_{rO} - B_1 \sigma_{rI} = x(t), \quad (19)$$

$$\frac{d\sigma_{rI}}{dt} - B_3 \sigma_{rI} - B_4 \sigma_{rO} = y(t), \quad (20)$$

where the quantities $B_i$ are determined from Eqs. (A.8)–(A.12) of the Appendix.

The functions $x(t)$ and $y(t)$ can be suitably represented over a time increment by the following linear functions in time:

$$x(t) = x_0 + x_1 t, \quad (21)$$

$$y(t) = y_0 + y_1 t. \quad (22)$$

The solution to Eqs. (19) and (20) becomes:

$$\sigma_{rO} = D_1 e^{m_1 t} + D_2 e^{m_2 t} + v_0 + v_1 t, \quad (23)$$

$$\sigma_{rI} = \frac{m_1 - B_2}{B_1} D_1 e^{m_1 t} + \frac{m_2 - B_2}{B_1} D_2 e^{m_2 t} + w_0 + w_1 t, \quad (24)$$

where $x_0$, $x_1$, $y_0$, $y_1$, $m_1$, $m_2$, $v_0$, $v_1$, $w_0$, and $w_1$ are given by Eqs. (A.13)–(A.21). These quantities are constant during a time increment, but change from one increment to the next.

Eqs. (19) and (20) apply to a three-layer system where there are two interface surfaces. This method of solution, though, can be applied as well to a system with any number of coating layers. The result is a set of simultaneous differential equations of the form of Eqs. (19) and (20), where there is an equation for each interface surface. These can be solved using matrix analysis, which yields a set of eigenvalues and eigenvectors for the system. The eigenvalues for the two-equation system above are $m_1$ and $m_2$.

As discussed above, the solution is applied in time increments, which means that coefficients $D_1$ and $D_2$ for each increment are determined from the initial conditions for that increment. At the start of irradiation ($t = 0$), the initial values for internal pressure $p$ and external pressure $q$ are applied. At $t = 0$, all integral terms in Eqs. (15)–(18) vanish, and the equations are readily solved to give the following for the radial interface stresses at the start of irradiation:

$$\sigma_{rO}(0) = \frac{a_1 c_1 p - d_2 (b_1 - a_2) q}{b_2 c_1 - (c_2 - d_1)(b_1 - a_2)}, \quad (25)$$

$$\sigma_{rI}(0) = \frac{a_1 (c_2 - d_1) p - d_2 b_2 q}{(b_1 - a_2)(c_2 - d_1) - c_1 b_2}. \quad (26)$$

These become the initial conditions for determining the coefficients $D_1$ and $D_2$ for the first increment. In subsequent time increments, the radial stresses at the end of an increment become the initial conditions for the next increment. Using Eqs. (23) and (24), then, the coefficients for the general time increment $n$ are determined to be

$$D_1 = \frac{(m_2 - B_2) X - B_1 Y}{m_2 - m_1} e^{-m_1 t_{n-1}}, \quad (27)$$

$$D_2 = \frac{(m_1 - B_2) X - B_1 Y}{m_1 - m_2} e^{-m_2 t_{n-1}}, \quad (28)$$

where

$$X = \sigma_{rO}(t_{n-1}) - v_0 - v_1 t_{n-1}, \quad (29)$$

$$Y = \sigma_{rI}(t_{n-1}) - w_0 - w_1 t_{n-1} \quad (30)$$

and $t_{n-1}$ denotes the time $t$ at the end of the previous increment $n - 1$. In applying these equations, all material properties, swelling strain rates, thermal expansion strain rates, and known internal and external pressures are numerically averaged over the time increment.

### 2.3. Function $F(t)$

Substituting Eq. (10) into (11) and differentiating with respect to $t$ gives the following equation for the function $F(t)$:

$$\frac{dF}{dt} + \frac{cE(1 - \nu)}{1 - \mu} F = \frac{E}{1 - \mu} (\overline{S}_r + \overline{\alpha}_r \overline{\dot{T}} - \overline{S}_t - \overline{\alpha}_t \overline{\dot{T}}). \quad (31)$$

The overbars in Eq. (31) serve as a reminder that swelling and thermal expansion strain rates are numerically averaged over the time increment, and are treated as constants through the increment. The general solution to this differential equation is

$$F(t) = [F(t_{n-1}) - a_0]e^{-\frac{cE(1-v)}{1-\mu}(t-t_{n-1})} + a_0, \tag{32}$$

where $a_0$ for time increment $n$ is

$$a_0 = \frac{\overline{S} + \overline{\alpha}_r\overline{T} - \overline{S}_t - \overline{\alpha}_t\overline{T}}{c(1-v)}. \tag{33}$$

There is a function $F(t)$ for each of the pyrocarbon layers. If the SiC layer is treated as an isotropic elastic medium, its $F(t)$ becomes zero.

### 2.4. General stress equations

Eqs. (23) and (24) give the radial contact stresses at the inside and outside surfaces of the SiC layer. Once these have been solved, together with $F(t)$ from Eq. (32), it is possible to determine radial or tangential stresses at any radial location in the coating layers. Tangential stresses are needed to determine whether the coating layers fail. Though the maximum value for tangential stress often occurs at the inner surface of the layer, there are times when the maximum stress in a pyrocarbon layer occurs at the outer surface. As in Ref. [9], the following general expressions for radial and tangential stresses in a coating layer can be developed:

$$\sigma_r(r,t) = \frac{r_a^3(r_b^3 - r^3)}{r^3(r_b^3 - r_a^3)}p - \frac{r_b^3(r_a^3 - r^3)}{r^3(r_b^3 - r_a^3)}q - \frac{2}{3}\left[\frac{r_a^3(r_b^3 - r^3)\ln r_a - r_b^3(r_a^3 - r^3)\ln r_b}{r^3(r_b^3 - r_a^3)} - \ln r\right]F(t), \tag{34}$$

$$\sigma_t(r,t) = -\frac{r_a^3(2r^3 + r_b^3)}{2r^3(r_b^3 - r_a^3)}p - \frac{r_b^3(2r^3 + r_a^3)}{2r^3(r_b^3 - r_a^3)}q + \frac{1}{3}\left[\frac{r_a^3(r_b^3 + 2r^3)\ln r_a - r_b^3(r_a^3 + 2r^3)\ln r_b}{r^3(r_b^3 - r_a^3)} + 2\ln r + 1\right]F(t), \tag{35}$$

where $r_a$ and $r_b$ are the inner and outer radii of the layer, respectively, and $p$ and $q$ are the radial stresses acting on the inner and outer surfaces of the layer, respectively. Unlike the $F(t)$ of Ref. [9], that of Eq. (32) allows Poisson's ratio in creep ($v$) to be set to any value.

## 3. Displacements

Displacements are calculated at the radial locations $r_2$, $r_3$, $r_4$, and $r_5$ so that new values can be determined for these radii at the end of each time increment. The updated radii are needed in the thermal and fission product transport analyses of the particle, and can also be used in the stress solution. Once the radial stresses $\sigma_{rO}$ and $\sigma_{rI}$ are determined, then the displacements at the inner and outer surfaces of the SiC are determined from Eqs. (16) and (17). Because of the integrations in these equations, the displacements are most readily determined by differentiating through with respect to $t$, and calculating the displacements incrementally. For example, Eq. (16) becomes

$$\Delta u_I = b_1\Delta\sigma_{rI} + b_2\Delta\sigma_{rO} + b_3\alpha_{rS}\dot{T}_S\Delta t + b_4\alpha_{tS}\dot{T}_S\Delta t. \tag{36}$$

The displacements at $r_2$ and $r_5$ are obtained from Eqs. (15) and (18), except that the coefficients are modified appropriately and the equations are applied incrementally. These become

$$\Delta u_2 = a_1'\Delta p + a_2'\Delta\sigma_{rI} + (a_3'p + a_4'\sigma_{rI})c_I\Delta t + a_5'(S_{rI} + \alpha_{rI}\dot{T}_I)\Delta t + a_6'(S_{tI} + \alpha_{tI}\dot{T}_I)\Delta t, \tag{37}$$

$$\Delta u_5 = d_1'\Delta\sigma_{rO} + d_2'\Delta q + (d_3'\sigma_{rO} + d_4'q)c_O\Delta t + d_5'(S_{rO} + \alpha_{rO}\dot{T}_O)\Delta t + d_6'(S_{tO} + \alpha_{tO}\dot{T}_O)\Delta t. \tag{38}$$

The coefficients $a_i'$ and $d_i'$ are calculated from Eqs. (A.1)–(A.6) using dimensions appropriate for the IPyC inner surface and OPyC outer surface, respectively.

An important aspect of the fuel particle behavior is the development of a gap between the buffer and IPyC layers during irradiation. The gap is formed because the irradiation-induced shrinkage of the porous buffer exceeds that of the IPyC layer. A significant consequence of this gap is that the low thermal conductivity of the gap region (which is occupied by fission products) contributes to an increase in the kernel temperature. The kernel temperature affects fission gas release, which in turn affects the gas pressure acting on the coating layers and fission product transport through the particle layers and fuel matrix. Because the magnitude of the increase in kernel temperature depends on the size of the gap, PARFUME calculates the gap size throughout irradiation. This is done by calculating a displacement for the outer surface of the buffer layer in addition to displacement $u_2$ of the IPyC inner surface. In this calculation, the buffer is assumed to shrink and creep due to irradiation and the fuel kernel is assumed to swell throughout irradiation. It is currently assumed in PARFUME that the inner surface of the buffer moves with the kernel, and that the buffer remains intact throughout irradiation. Application of Eq. (14) to the inner surface of the buffer gives the following:

$$p_B = \frac{1}{a_{1B}}\left[u_k - a_{3B}\int p_B c_B\,dt - r_1\int(S_B + \alpha_B\dot{T})\,dt\right], \tag{39}$$

where $p_B$ is the radial contact stress at the interface of the kernel and buffer; $u_k$ is the known displacement of the kernel surface; and $c_B$, $S_B$, and $\alpha_B$ are creep, shrinkage, and expansion properties for the buffer. The coefficients $a_{1B}$ and $a_{3B}$ are obtained by substituting appropriate values into Eqs. (A.1) and (A.3). Because of its porosity, the buffer is assumed to experience no deformation due to the gas pressure. Thus, there is no pressure applied to its outer

surface. Also, because the buffer is assumed to be isotropic (per Ref. [7], for low-density pyrocarbon), the radial components of swelling and thermal expansion strain rate $(S, \alpha\dot{T})$ are set equal to the corresponding tangential components.

The pressure $p_B$ can be determined from Eq. (39) by differentiating through with respect to $t$, and solving the resulting differential equation. This gives the following for the pressure at any time during time increment $n$:

$$p_B(t) = \left\{ p_B(t_{n-1}) - \frac{1}{a_{3B}c_B}\left[\frac{du_k}{dt} - r_1(S_B + \alpha_B\dot{T})\right]\right\} e^{-\frac{a_{3B}}{a_{1B}}c(t-t_{n-1})} + \frac{1}{a_{3B}c_B}\left[\frac{du_k}{dt} - r_1(S_B + \alpha_B\dot{T})\right], \tag{40}$$

where $t_{n-1}$ is the time at the start of the increment, and the derivative $du_k/dt$ is treated as a constant through the time increment. Using this contact pressure, the displacement at the outer surface of the buffer ($u_{2B}$) is then determined incrementally from

$$\Delta u_{2B} = b_{1B}\Delta p_B + b_{3B}p_B c_B \Delta t + r_{2B}(S_B + \alpha_B\dot{T})\Delta t, \tag{41}$$

where $b_{1B}$ and $b_{3B}$ are determined from Eqs. (A.1) and (A.3) using dimensions at the outer surface of the buffer, and $r_{2B}$ is the outer radius of the buffer.

## 4. Two-layer and one-layer solutions

Situations arise in fuel particle evaluations that require stress analysis of a two-layer or one-layer shell. For example, a detachment of the IPyC from the SiC results in both two-layer (SiC/OPyC) and one-layer (IPyC) shells. In such cases, an assessment is made as to whether the IPyC shell can sustain the internal pressure on its own. If it fails, then the internal pressure is applied directly to the two-layer (SiC/OPyC) shell. Stresses and displacements for a two-layer shell are obtained in the same manner as used for the three-layer shell, i.e. by equating displacements at the interface between layers to solve for the radial stress at the interface. This contact stress, together with the known internal and external pressures, is used to determine displacements at the layer surfaces. The tangential stresses in the layers are determined using Eq. (35) [and Eq. (32) for $F(t)$].

The radial stress at the SiC/OPyC interface for a particle having a debonded IPyC is as follows:

$$\sigma_{rO} = D'_1 e^{m'_1 t} - \frac{x'_0 + x'_1}{m'_1} - \frac{x'_1}{m'_1}t, \tag{42}$$

while the radial stress at the IPyC/SiC interface for a particle having a debonded OPyC is

$$\sigma_{rI} = D'_2 e^{m'_2 t} - \frac{y'_0 + y'_1}{m'_2} - \frac{y'_1}{m'_2}t, \tag{43}$$

where the primed quantities are determined from Eqs. (A.22)–(A.29).

Since there is no radial interface stress to calculate in a one-layer particle, the known internal and external pres-

Table 1
Input parameters for benchmark case

| Parameter | Units | Value |
|---|---|---|
| *Fuel characteristics* | | |
| Oxygen-to-uranium ratio | Atom ratio | 2 |
| Carbon-to-uranium ratio | Atom ratio | 0 |
| U-235 enrichment | wt% | 10 |
| Kernel diameter | μm | 500 |
| Buffer thickness | μm | 100 |
| IPyC thickness | μm | 40 |
| SiC thickness | μm | 35 |
| OPyC thickness | μm | 40 |
| Kernel density | $Mg/m^3$ | 10.8 |
| Buffer density | $Mg/m^3$ | 0.95 |
| IPyC density | $Mg/m^3$ | 1.90 |
| SiC density | $Mg/m^3$ | 3.20 |
| OPyC density | $Mg/m^3$ | 1.90 |
| IPyC BAF | | 1.03 |
| OPyC BAF | | 1.03 |
| PyC and buffer Poisson's ratio in creep | | 0.5 |
| PyC elastic Poisson's ratio | | 0.33 |
| PyC creep coefficient | $(MPa\ 10^{25}\ n/m^2)^{-1}$ $E > 0.18$ MeV | $1.765 \times 10^{-4}$ @ 1073 K (varies) |
| PyC Young's modulus | MPa | $3.96 \times 10^4$ |
| SiC elastic Poisson's ratio | | 0.13 |
| SiC Young's modulus | MPa | $3.70 \times 10^5$ |
| PyC tangential swelling strain rate | $(10^{25}\ n/m^2)^{-1}$ | −0.00903 @ $t = 2 \times 10^{25}\ n/m^2$ (varies) |
| PyC thermal expansion strain rate | $(10^{25}\ n/m^2)^{-1}$ | 0.00713 |
| *Irradiation conditions* | | |
| Irradiation duration | Effective full power days | 1000 |
| End-of-life burnup | % FIMA | 10 |
| End-of-life fluence | $10^{25}\ n/m^2$, $E > 0.18$ MeV | 3 |
| Temperature at outer surface of OPyC layer | K | 873–1273 (10 cycles) |
| Ambient pressure | MPa | 0.1 |

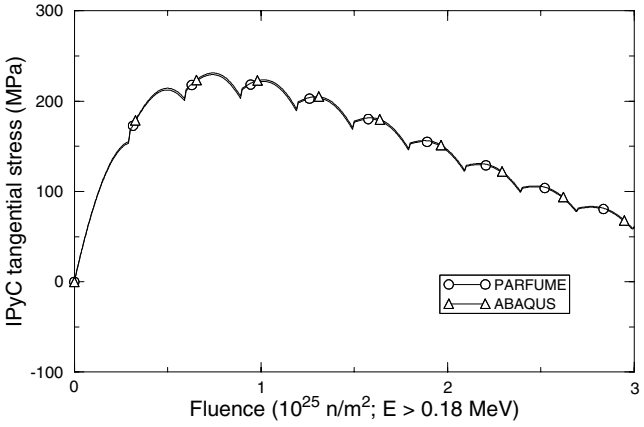


Fig. 3. Comparison of PARFUME and ABAQUS maximum IPyC tangential stress histories in benchmark case.

sures acting on the layer can be used directly to determine displacements and tangential stresses.

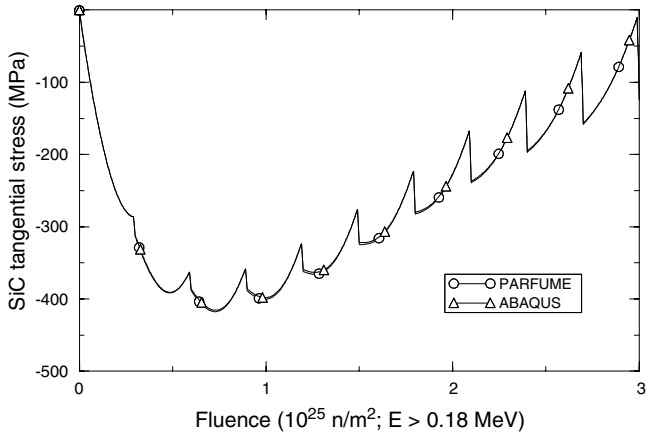


Fig. 4. Comparison of PARFUME and ABAQUS maximum SiC tangential stress histories in benchmark case.

Table 2
Input parameters for example problem

| Parameter | Units | Value |
|---|---|---|
| *Fuel characteristics* | | |
| Oxygen-to-uranium ratio | Atom ratio | 1.36 |
| Carbon-to-uranium ratio | Atom ratio | 0.33 |
| U-235 enrichment | wt% | 20 |
| Kernel diameter | μm | 350 |
| Buffer thickness | μm | 100 |
| IPyC thickness | μm | 40 |
| SiC thickness | μm | 35 |
| OPyC thickness | μm | 40 |
| Kernel density | Mg/m$^3$ | 10.66 |
| Buffer density | Mg/m$^3$ | 1.00 |
| IPyC density | Mg/m$^3$ | 1.90 |
| SiC density | Mg/m$^3$ | 3.20 |
| OPyC density | Mg/m$^3$ | 1.90 |
| IPyC BAF | | 1.02 |
| OPyC BAF | | 1.02 |
| Kernel swelling | % volume change per 1% burnup | 0.8 |
| PyC and buffer Poisson's ratio in creep | | 0.5 |
| PyC elastic Poisson's ratio | | 0.33 |
| PyC creep coefficient | (MPa $10^{25}$ n/m$^2$)$^{-1}$ $E > 0.18$ MeV | $4.93 \times 10^{-4}$ |
| PyC Young's modulus | MPa | $3.27 \times 10^4$ |
| SiC elastic Poisson's ratio | | 0.30 |
| SiC Young's modulus | MPa | $4.21 \times 10^5$ |
| PyC tangential swelling strain rate | ($10^{25}$ n/m$^2$)$^{-1}$ | $-0.0217$ @ $t = 2 \times 10^{25}$ n/m$^2$ (varies) |
| *Irradiation conditions* | | |
| Particle power | mW | 100 |
| End-of-life burnup | % FIMA | 20 |
| End-of-life fluence | $10^{25}$ n/m$^2$, $E > 0.18$ MeV | 4 |
| Temperature at outer surface of OPyC layer | K | 1273 |
| Ambient pressure | MPa | 0.1 |

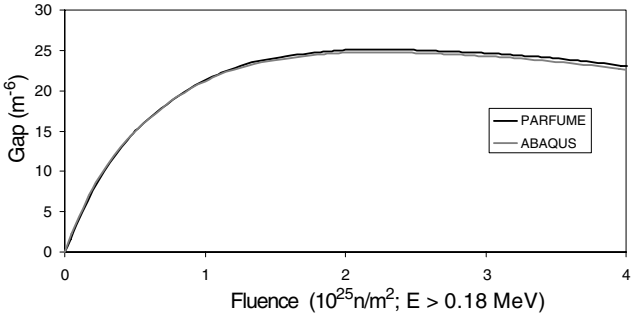


Fig. 5. Comparison between PARFUME and ABAQUS buffer/IPyC gap calculations.

## 5. Comparison with finite element analysis

As part of the International Atomic Energy Agency (IAEA) Coordinated Research Program (CRP), results obtained from PARFUME's derived solution have been benchmarked against ABAQUS [10] finite element results for a number of cases. In one of these, the irradiation temperature was cycled 10 times between the values of 873 and 1273 K, inducing differential thermal expansion between the layers. The internal pressure ratcheted upward from an initial value of 0 MPa to a peak value of 26.13 MPa. Input parameters for this case are summarized in Table 1. The ABAQUS solution employed an axisymmetric model having five elements through the thickness of the IPyC layer, three elements through the SiC layer, and four elements through the OPyC layer.

The IPyC and SiC tangential stresses obtained from these solutions are compared in Figs. 3 and 4, which show very close agreement in the results. The accuracy of displacements calculated with the derived solution is assessed by comparing the calculated buffer/IPyC gap size with ABAQUS results in an example problem. The input parameters for the particle selected for this analysis are presented in Table 2. The buffer was assumed to remain intact and bonded to the kernel. As shown in Fig. 5, there is again close agreement in results.

## 6. Conclusion

A closed-form solution for calculating stresses in TRISO-coated particles has been modified to remove several limitations in its application to fuel particle analysis. The modified solution is applied incrementally through irradiation, which allows the material properties and irradiation temperature to change with time. The incremental solution also facilitates the determination of a time history for the particle failure probability through irradiation. The solution also enables the calculation of displacements at each increment, which are used in thermal analysis to calculate fission gas pressure and particle temperatures. Furthermore, the modified solution relieves the requirement that Poisson's ratio in creep for the pyrocarbon layers be set at a value of 0.5. This solution has been implemented in the PARFUME fuel performance code, where it has

been demonstrated to perform efficiently in particle failure probability calculations.

## Acknowledgment

Work supported by the US Department of Energy, Office of Nuclear Energy, under DOE Idaho Operations Office Contract DE-AC07-05ID14517.

## Appendix

Equations for quantities contained in the derivations are

$$K_1 = -\frac{2r^3 r_a^3(1-2\mu) + r_a^3 r_b^3(1+\mu)}{2Er^2\left(r_b^3 - r_a^3\right)}, \tag{A.1}$$

$$K_2 = \frac{2r^3 r_b^3(1-2\mu) + r_a^3 r_b^3(1+\mu)}{2Er^2\left(r_b^3 - r_a^3\right)}, \tag{A.2}$$

$$K_3 = -\frac{r_a^3 r_b^3(1+\nu) + 2r^3 r_a^3(1-2\nu)}{2r^2\left(r_b^3 - r_a^3\right)}, \tag{A.3}$$

$$K_4 = \frac{r_a^3 r_b^3(1+\nu) + 2r^3 r_b^3(1-2\nu)}{2r^2\left(r_b^3 - r_a^3\right)}, \tag{A.4}$$

$$K_5 = \frac{r_a^3 r_b^3 \ln\frac{r_a}{r_b}}{r^2\left(r_b^3 - r_a^3\right)} + \frac{r}{3}, \tag{A.5}$$

$$K_6 = -\frac{r_a^3 r_b^3 \ln\frac{r_a}{r_b}}{r^2\left(r_b^3 - r_a^3\right)} + \frac{2r}{3}, \tag{A.6}$$

$$K_7 = \frac{2(\nu-\mu)}{3E(\nu-1)}\left[\frac{r_b^3\left(r^3 - r_a^3\right)\ln r_b - r_a^3\left(r^3 - r_b^3\right)\ln r_a}{r^2\left(r_b^3 - r_a^3\right)} - r\ln r\right], \tag{A.7}$$

$$Z = b_2 c_1 - (c_2 - d_1)(b_1 - a_2), \tag{A.8}$$

$$B_1 = \frac{a_4 c_I c_1}{Z}, \tag{A.9}$$

$$B_2 = -\frac{d_3 c_O (b_1 - a_2)}{Z}, \tag{A.10}$$

$$B_3 = -\frac{a_4 c_I (c_2 - d_1)}{Z}, \tag{A.11}$$

$$B_4 = \frac{d_3 c_O b_2}{Z}, \tag{A.12}$$

$$\begin{aligned} x_0 Z = {} & [-c_1 r_3 + (b_1 - a_2) r_4]\overline{\alpha}_S \frac{\Delta T_S}{\Delta t} + a_1 c_1 \frac{\Delta p}{\Delta t} \\ & - d_2(b_1 - a_2)\frac{\Delta q}{\Delta t} + c_1 a_3 c_I\left(p_{n-1} - \frac{\Delta p}{\Delta t} t_{n-1}\right) \\ & - d_4(b_1 - a_2) c_O\left(q_{n-1} - \frac{\Delta q}{\Delta t} t_{n-1}\right) \\ & + a_5 c_1\left(\overline{S}_{rI} + \overline{\alpha}_{rI}\frac{\Delta T_I}{\Delta t}\right) + a_6 c_1\left(\overline{S}_{tI} + \overline{\alpha}_{tI}\frac{\Delta T_I}{\Delta t}\right) \\ & - d_5(b_1 - a_2)\left(\overline{S}_{rO} + \overline{\alpha}_{rO}\frac{\Delta T_O}{\Delta t}\right) \\ & - d_6(b_1 - a_2)\left(\overline{S}_{tO} + \overline{\alpha}_{tO}\frac{\Delta T_O}{\Delta t}\right), \end{aligned} \tag{A.13}$$

$$x_1 = \frac{1}{Z}\left[c_1 a_3 c_I \frac{\Delta p}{\Delta t} - d_4(b_1 - a_2) c_O \frac{\Delta q}{\Delta t}\right], \tag{A.14}$$

$$\begin{aligned} -y_0 Z = {} & [b_2 r_4 - (c_2 - d_1) r_3]\overline{\alpha}_S \frac{\Delta T_S}{\Delta t} + a_1(c_2 - d_1)\frac{\Delta p}{\Delta t} \\ & - b_2 d_2 \frac{\Delta q}{\Delta t} + a_3(c_2 - d_1) c_I\left(p_{n-1} - \frac{\Delta p}{\Delta t} t_{n-1}\right) \\ & - b_2 d_4 c_O\left(q_{n-1} - \frac{\Delta q}{\Delta t} t_{n-1}\right) \\ & + a_5(c_2 - d_1)\left(\overline{S}_{rI} + \overline{\alpha}_{rI}\frac{\Delta T_I}{\Delta t}\right) \\ & + a_6(c_2 - d_1)\left(\overline{S}_{tI} + \overline{\alpha}_{tI}\frac{\Delta T_I}{\Delta t}\right) \\ & - b_2 d_5\left(\overline{S}_{rO} + \overline{\alpha}_{rO}\frac{\Delta T_O}{\Delta t}\right) - b_2 d_6\left(\overline{S}_{tO} + \overline{\alpha}_{tO}\frac{\Delta T_O}{\Delta t}\right), \end{aligned} \tag{A.15}$$

$$y_1 = -\frac{1}{Z}\left[a_3(c_2 - d_1) c_I \frac{\Delta p}{\Delta t} - b_2 d_4 c_O \frac{\Delta q}{\Delta t}\right], \tag{A.16}$$

$$m_1, m_2 = \frac{1}{2}\left\{B_2 + B_3 \pm \sqrt{(B_2 + B_3)^2 - 4(B_2 B_3 - B_1 B_4)}\right\}, \tag{A.17}$$

$$v_1 = \frac{B_1 y_1 - B_3 x_1}{B_2 B_3 - B_1 B_4}, \tag{A.18}$$

$$v_0 = \frac{(B_2 + B_3) v_1 + x_1 - B_3 x_0 + B_1 y_0}{B_2 B_3 - B_1 B_4}, \tag{A.19}$$

$$w_0 = \frac{1}{B_1}(v_1 - B_2 v_0 - x_0), \tag{A.20}$$

$$w_1 = -\frac{B_2 v_1 + x_1}{B_1}, \tag{A.21}$$

$$\begin{aligned} x_0'(c_2 - d_1) = {} & -(c_3 + c_4)\overline{\alpha}_S \frac{\Delta T_S}{\Delta t} + d_2 \frac{\Delta q}{\Delta t} + d_4 c_O\left(q - \frac{\Delta q}{\Delta t} t_{n-1}\right) \\ & + d_5\left(\overline{S}_{rO} + \alpha_{rO}\frac{\Delta T_O}{\Delta t}\right) + d_6\left(\overline{S}_{tO} + \overline{\alpha}_{tO}\frac{\Delta T_O}{\Delta t}\right) - c_1 \frac{\Delta p}{\Delta t}, \end{aligned} \tag{A.22}$$

$$x_1' = \frac{1}{c_2 - d_1} d_4 c_O \frac{\Delta q}{\Delta t}, \tag{A.23}$$

$$\begin{aligned} y_0'(b_1 - a_2) = {} & -(b_3 + b_4)\overline{\alpha}_S \frac{\Delta T_S}{\Delta t} + a_1 \frac{\Delta p}{\Delta t} + a_3 c_I\left(p - \frac{\Delta p}{\Delta t} t_{n-1}\right) \\ & + a_5\left(\overline{S}_{rI} + \alpha_{rI}\frac{\Delta T_I}{\Delta t}\right) + a_6\left(\overline{S}_{tI} + \overline{\alpha}_{tI}\frac{\Delta T_I}{\Delta t}\right) - b_2 \frac{\Delta q}{\Delta t}, \end{aligned} \tag{A.24}$$

$$y_1' = \frac{1}{b_1 - a_2} a_3 c_I \frac{\Delta p}{\Delta t}, \tag{A.25}$$

$$m_1' = \frac{d_3 c_O}{c_2 - d_1}, \tag{A.26}$$

$$m_2' = \frac{a_4 c_I}{b_1 - a_2}, \tag{A.27}$$

$$D_1' = \left[\sigma_{rO}(t_{n-1}) + \frac{x_0' + x_1'}{m_1'} + \frac{x_1'}{m_1'} t_{n-1}\right] e^{-m_1' t_{n-1}}, \tag{A.28}$$

$$D_2' = \left[\sigma_{rI}(t_{n-1}) + \frac{y_0' + y_1'}{m_2'} + \frac{y_1'}{m_2'} t_{n-1}\right] e^{-m_2' t_{n-1}}. \tag{A.29}$$

Thermal expansion in the SiC layer, represented by $\alpha_S \Delta T_S$, is assumed to be isotropic in this Appendix.

## References

[1] J.L. Kaae, J. Nucl. Mater. 32 (1969) 322.
[2] H. Walther, Nucl. Eng. Des. 18 (1971) 11.
[3] K. Bongartz, Status of the Fuel Stress and Failure Rate Calculations at KFA, JUL-1686, KFA Julich, GmbH, 1980.
[4] G.K. Miller, R.G. Bennett, J. Nucl. Mater. 206 (1993) 35.
[5] J.L. Kaae, Carbon 12 (1974) 577.
[6] I.S. Sokolnikoff, Mathematical Theory of Elasticity, 2nd Ed., McGraw-Hill, New York, 1956, p. 184.
[7] NP-MHTGR Material Models of Pyrocarbon and Pyrolytic Silicon Carbide, CEGA Corporation, CEGA-002820, Rev. 1 July 1993.
[8] D.G. Martin, Nucl. Eng. Des. 213 (2002) 241.
[9] G.K. Miller, Int. J. Solids Struct. 32 (14) (1995) 2007.
[10] ABAQUS Analysis User's Manual, Version 6.4, 2003.